Latin American Journal of Solids and Structures
www.lajss.org

Transient Stress Intensity Factors of Functionally Graded Hollow Cylinders with Internal Circumferential Cracks

Abstract

In this paper, transient thermomechanical stress intensity factors for functionally graded cylinders with complete internal circumferential cracks are obtained using the weight function method. The finite difference method is used to calculate the time dependent temperature distribution and thermal stresses along the cylinder thickness. Furthermore, finite element analysis is performed to determine the weight function coefficients and to investigate the accuracy of the predicted stress intensity factors from the weight functions. Variation of the stress intensity factors with time and effects of the material gradation on the results are investigated, as well. It is shown that the proposed technique can be used to accurately predict transient thermomechanical stress intensity factors for functionally graded cylinders with arbitrary material gradation.

Keywords

Fracture; circumferential crack; functionally graded materials; hollow cylinder; transient analysis.

Iman Eshraghi [a,*]
Nasser Soltani [b,*]
Mohammad Rajabi [c,*]

[a] Email: ieshraghi@ut.ac.ir (Corresponding Author)
[b] Email: nsoltani@ut.ac.ir
[c] Email: mohammad.rajabi@ut.ac.ir
[*]Intelligence Based Experimental Mechanics Center, Department of Mechanical Engineering, College of Engineering, University of Tehran, Tehran, Iran.

http://dx.doi.org/10.1590/1679-78252217

Received 17.06.2015
Accepted 09.04.2016
Available online 12.04.2016

1 INTRODUCTION

Functionally graded materials (FGMs), as a new class of composite materials, have smooth variation for their material properties along one or more spatial directions. Improved performance of the thermal and mechanical properties of FGMs has led to many different applications of them. These applications include, but not limited to, thermal barrier coatings (Baig et al. 2014), biomaterials (Afzal et al. 2012), wear resistant cutting tools (Garcia & Pitonak 2013), and micro-electro-mechanical-systems (MEMS) (Eshraghi et al. 2015). Cylindrical structures made of FGMs have applications in the aerospace and the automotive industries, as well (Han et al. 2001). In many of these applications, the cylinder may be subject to transient thermal loads which can result in mechanical and/or thermal stresses in the structure. Such transient thermal and/or mechanical stresses are equal to or higher than those of the corresponding steady state operation. Thus, the steady state and transient thermo-

elastic problems of hollow and solid cylinders made from FGMs have been the subject of research for years (Shao & Ma 2008; Liew et al. 2003; Peng & Li 2010; Lee et al. 2012; Gharooni et al. 2016).

Presence of small cracks, for example cracks at weld locations, can result in early crack growth and final leakage or failure of the structure subject to thermomechanical loads. In addition, transient thermomechanical cycles can result in the fatigue of the structure (Ando et al. 2013). In this regard, structural integrity assessment of the structure is necessary to ensure its safe operation. Among various combinations of crack orientation and location, circumferential cracks are often seen at the joint sections of pipelines and pressure vessels mostly because of the incomplete penetration of the weld material into the interface. Therefore, fracture analysis of homogeneous cylindrical geometries with circumferential cracks has been the subject of works of many researches in past decades (Meshii et al. 2006; Nabavi & Ghajar 2010; Nied & Erdogan 1983; Grebner 1985).

The problem of cracked FG cylinders has also been analytically and numerically studied by few researchers. For example, Afsar and Anisuzzaman (Afsar & Anisuzzaman 2007) considered the problem of thick-walled pressurized FG cylinders with two diametrically-opposed edge cracks. They modeled the FG cylinder with an equivalent homogeneous cylinder with induced thermal strains as a result of cooling from sintering temperature and internal pressure. In another work, Afsar et al. (Afsar et al. 2009) identified the optimum material distribution for a thick-walled FG cylinder with two diametrically opposed internal cracks in order to obtain desired fracture characteristics. Nami and Eskandari (Nami & Eskandari 2012a; Nami & Eskandari 2012b) used three-dimensional finite element (FE) modeling to derive SIFs for FG cylinders with semi-elliptical circumferential surface cracks subject to thermal and mechanical loadings. They showed that the crack geometry and the material gradation have considerable effect on the SIF distribution in front of the crack.

In most of the published works on the analysis of cracked FG structures, analytical methods (Guo & Noda 2014), energy methods combined with the standard FE analysis (Walters et al. 2006; Zhang et al. 2014), or the extended finite element method (XFEM) (Bayesteh & Mohammadi 2013) have been used for the calculation of SIFs. Analytical approaches are limited to specific (and often simple) geometries and loading conditions. The energy methods require separate FE modeling and analysis for each loading condition and each crack configuration which is often time consuming. The weight function method, on the other hand, is an efficient approach for the calculation of SIFs. For example, the weight function method based on the direct adjustment scheme (Fett 1992) requires knowledge of finite number of reference SIFs. These reference SIFs can be obtained using any analytical or numerical method (including the FE method) and the weight function coefficients can be calculated from the obtained reference SIF results. Once the weight function coefficients are determined, SIFs for any loading condition can be easily obtained with a simple integration procedure. This method has been widely used in past to obtain mechanical and/or thermal SIFs of homogeneous cylinders (Shahani & Nabavi 2007; Shahani & Nabavi 2006; Ghajar & Nabavi 2010).

When it comes to the application of the weight function method to FG cracked structures, the combination of the weight function method and the energy-based FE method minimizes the number of required FE analysis for a given crack geometry with different loading conditions (Fett et al. 2000a; Fett et al. 2000b). Bahr et al. (Bahr et al. 2003) applied the weight function method to determine SIFs in FG structures with residual stresses. Shi et al. (Shi et al. 2014) proposed basic weight function equations for two-dimensional FG cracked structures using Betti's reciprocal theorem. Seifi (Seifi

2015) calculated residual stresses for autofrettaged FG cylinders and obtained SIFs at the deepest and surface breaking points of a semi-elliptical axial crack using the weight function approach. The first two authors have applied the weight function method to FG cylinders with internal circumferential cracks under mechanical and thermal loads and have shown the accuracy of the method in predicting the SIFs (Eshraghi & Soltani 2015a; Eshraghi & Soltani 2015b). A domain form of the *J*-integral for axisymmetric FG cylinders was used in their works to obtain reference SIFs from the FE analysis results.

The problem of hollow FG cylinders with internal circumferential cracks subject to transient thermomechanical loads has not been considered in the literature, yet. More specifically, to the best of the authors' knowledge, the weight function method has not been used to study this problem. The weight function method, as a simple, accurate, and computationally efficient method, can be used to study the transient behavior of FG cracked cylinders under thermomechanical loads. Applicability of the weight function method to FG cylinders with internal circumferential cracks subject to mechanical loads was previously studied and validated by the first two authors (Eshraghi & Soltani 2015a). In this work, we use the weight function expressions given in (Glinka & Shen 1991) to calculate the transient thermomechanical SIFs of circumferential cracks in FG cylinders. The FG cylinder is under internal and external pressure loads as well as internal and external convection heat transfer. No specific material gradation profile is pre-assumed in the analysis for derivation and integration of the governing equations. The governing equations for the cylinder temperature distribution and the corresponding radial displacement component are discretized and numerically solved using the finite difference method. Using the weight function expression and the axial component of the thermal stress, mode-I thermomechanical SIF of FG cracked cylinders is obtained. The weight function coefficients are determined using reference SIF results obtained from the FE analyses for three reference crack surface loads. The domain form of the *J*-integral for axisymmetric FG structures is implemented in the post-processing step of the FE analysis to calculate the reference SIFs. Numerical results are presented for a FG cylinder that its thermomechanical properties vary through the wall thickness based on a power law scheme. Furthermore, for this specific material gradation profile, a mathematical expression is fitted to the SIFs extracted from FE results. This mathematical expression can be used to calculate reference SIFs for different values of crack depth to cylinder thickness ratio and different FG power law index values with no need for any additional FE analysis. Comparison of the predicted thermal SIF results by the presented weight function method with those of the direct FE analysis results shows the applicability of the presented weight function method for accurate prediction of SIFs of cracked FG cylinders under thermo-mechanical loads. Effects of the crack depth to cylinder wall thickness ratio and the FG power law index on the transient thermomechanical SIF results are discussed, as well.

2 TRANSIENT THERMAL STRESS ANALYSIS OF FG HOLLOW CYLINDERS

As shown in Fig. 1, an infinitely long thick-walled cylinder with inner radius r_i and outer radius r_o, has a complete internal circumferential crack of depth a. Convection heat transfer exists at the inner and the outer surfaces of the cylinder with constant convection heat transfer coefficients h_i and h_o and fluid temperatures T_i and T_o, respectively. Internal pressure p_i and external pressure p_o are

applied to the inner and the outer surfaces of the cylinder, respectively, as well. Thermomechanical material properties vary along the wall thickness of the FG cylinder. The governing equations and the associated boundary conditions of the problem described in Fig. 1, in the absence of the circumferential crack, will be presented in what follows.

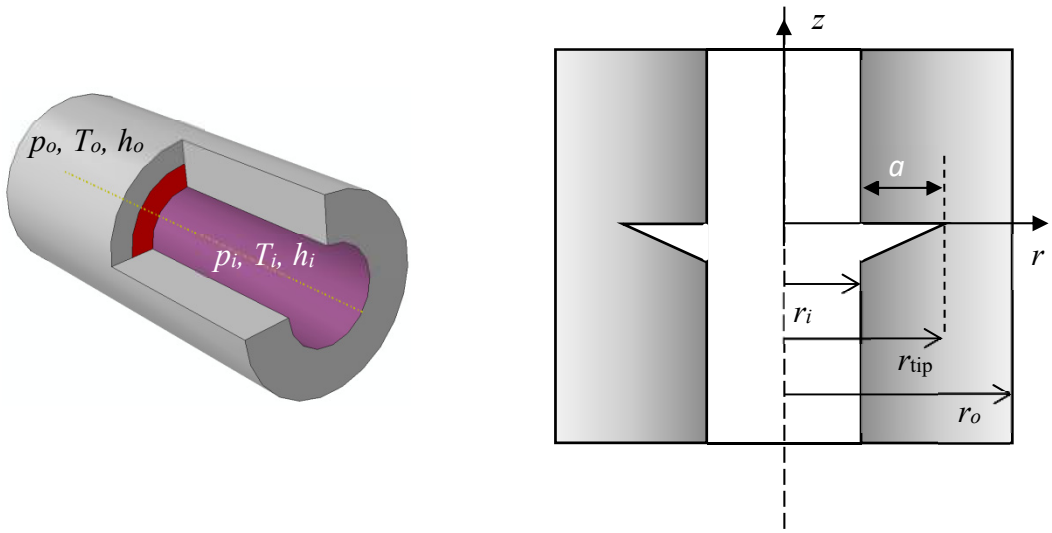

Figure 1: Schematic of a circumferential crack in a pressurized cylinder subject to transient thermal loads.

2.1 Governing Equations and Boundary Conditions of Transient Thermal Analysis

If the coupling term in the energy equation is neglected, the one-dimensional axisymmetric transient heat conduction equation for the above hollow FG cylinder can be written as (Shao et al. 2007)

$$c(r)\rho(r)\frac{\partial T(r,t)}{\partial t} = \frac{1}{r}\frac{\partial}{\partial r}\left[rk(r)\frac{\partial T(r,t)}{\partial r}\right] \tag{1}$$

where $T(r,t)$ is the temperature of any material point in the cylinder with radial coordinate r at time t. All material properties, including thermal conductivity k, specific heat c, density ρ, the cylinder elastic module E, the cylinder Poisson's ratio ν, and the cylinder thermal expansion coefficient α, are assumed to vary along the radial direction. The initial and boundary thermal conditions at the inner and the outer surfaces of the cylinder are given by

$$T(r,0) = T_{\text{init}} \tag{2-a}$$

$$k_i\left[\frac{\partial T(r,t)}{\partial r}\right]_{r=r_i} = h_i\left[T(r_i,t) - T_i\right] \tag{2-b}$$

$$k_o\left[\frac{\partial T\left(r,t\right)}{\partial r}\right]_{r=r_o} = h_o\left[T_o - T\left(r_o,t\right)\right] \tag{2-c}$$

Where $T(r_i,t)$ and $T(r_o,t)$ represent time-dependent temperatures of the inner and the outer surfaces of the cylinder, respectively, and T_{init} is the uniform initial temperature of the cylinder. k_i and k_o are the thermal conductivity values of the FG material at the inner and the outer surfaces of the cylinder, respectively. The following dimensionless variables are defined in order to simplify the analysis and presentation of results.

$$\left(R,R_i,R_o\right) = \frac{\left(r,r_i,r_o\right)}{r_{ref}},\ \left(\theta,\theta_i,\theta_o\right) = \frac{\left(T,T_i,T_o\right) - T_{\text{init}}}{T_{ref}}, \tag{3-a}$$

$$\overline{c} = \frac{c}{c_{ref}},\ \overline{\rho} = \frac{\rho}{\rho_{ref}},\ \overline{k} = \frac{k}{k_{ref}}, \tag{3-b}$$

$$\tau = \frac{\chi_{ref}t}{r_{ref}^2}, \tag{3-c}$$

$$\left(\overline{h}_i,\overline{h}_o\right) = \frac{r_{ref}}{k_{ref}}\times\left(h_i,h_o\right),\ \left(H_i,H_o\right) = \left(\frac{\overline{h}_i}{\overline{k}_i},\frac{\overline{h}_o}{\overline{k}_o}\right) \tag{3-d}$$

where for any parameter subscript "*ref*" represents the arbitrary reference value of that parameter. In Eq. (3-c) χ_{ref} is given by $\chi_{ref} = k_{ref}/(c_{ref}\rho_{ref})$. Substitution of the dimensionless variables in Eq. (3) into Eqs. (1) and (2) yields the dimensionless forms of the governing equations and the initial and boundary conditions as:

$$\overline{c}\,\overline{\rho}\frac{\partial\theta}{\partial\tau} = \frac{1}{R}\frac{\partial}{\partial R}\left[R\overline{k}\frac{\partial\theta}{\partial R}\right] \tag{4}$$

and

$$\theta\left(R,0\right) = 0 \tag{5-a}$$

$$\left[\frac{\partial\theta}{\partial R} - H_i\theta\right]_{R=R_i} = -H_i\theta_i \tag{5-b}$$

$$\left[\frac{\partial\theta}{\partial R} + H_o\theta\right]_{R=R_o} = H_o\theta_o \tag{5-c}$$

2.2 Governing Equations and Boundary Conditions of Thermo-Elastic Analysis

With the help of the stress-strain relationship for a FG isotropic material and the equilibrium equation in the absence of body forces and neglecting the inertia effects, the governing equations for the thermo-elasticity problem of the cylinder is given as follows (Shao et al. 2007)

$$\left[1-\nu\left(r\right)\right]Z\left(r\right)\frac{\partial^2 u\left(r,t\right)}{\partial r^2}+\left\{\left[1-\nu\left(r\right)\right]\frac{dZ\left(r\right)}{dr}+\left[\frac{1-\nu\left(r\right)}{r}-\frac{d\nu\left(r\right)}{dr}\right]Z\left(r\right)\right\}\frac{\partial u\left(r,t\right)}{\partial r}$$

$$+\left\{\nu\left(r\right)\frac{dZ\left(r\right)}{dr}+\left[\frac{d\nu\left(r\right)}{dr}-\frac{1-\nu\left(r\right)}{r}\right]Z\left(r\right)\right\}\frac{u\left(r,t\right)}{r} \tag{6}$$

$$-\frac{d\left\{\left[1+\nu\left(r\right)\right]\alpha\left(r\right)Z\left(r\right)\right\}}{dr}\left[T\left(r,t\right)-T_{\text{init}}\right]-\left[1+\nu\left(r\right)\right]\alpha\left(r\right)Z\left(r\right)\frac{\partial T\left(r,t\right)}{\partial r}=0$$

Where $u(r,t)$ is the radial component of the displacement field. $E(r)$, $\nu(r)$, and $\alpha(r)$ are the cylinder elastic module, Poisson's ratio, and thermal expansion, respectively, and $Z\left(r\right)=\dfrac{E\left(r\right)}{\left[1+\nu\left(r\right)\right]\left[1-2\nu\left(r\right)\right]}$. Mechanical boundary conditions are prescribed pressures at the inner and the outer surfaces of the FG cylinder defined as follow

$$\sigma_r\left(r_i,t\right)=-p_i \tag{7-a}$$

$$\sigma_r\left(r_o,t\right)=-p_o \tag{7-b}$$

where $\sigma_r(r,t)$, is the radial stress component. For simplifying the analysis of the thermo-elastic problem of the hollow cylinder, the following dimensionless parameters are further defined.

$$U=\frac{u}{\alpha_{ref}T_{ref}r_{ref}},\ \left(\overline{\varepsilon}_r,\overline{\varepsilon}_\phi\right)=\frac{\left(\varepsilon_r,\varepsilon_\phi\right)}{\alpha_{ref}T_{ref}},\ \left(\overline{\sigma}_r,\overline{\sigma}_\phi,\overline{\sigma}_z\right)=\frac{\left(\sigma_r,\sigma_\phi,\sigma_z\right)}{E_{ref}\alpha_{ref}T_{ref}}, \tag{8-a}$$

$$\overline{E}=\frac{E}{E_{ref}},\ \overline{\alpha}=\frac{\alpha}{\alpha_{ref}},\ \zeta=\frac{Z}{E_{ref}}=\frac{\overline{E}}{\left(1+\nu\right)\left(1-2\nu\right)}, \tag{8-b}$$

$$\left(P_i,P_o\right)=\frac{\left(p_i,p_o\right)}{E_{ref}\alpha_{ref}T_{ref}} \tag{8-c}$$

Where $(\varepsilon_r, \varepsilon_\phi)$ are the radial and circumferential normal strains, respectively, and $(\sigma_r, \sigma_\phi, \sigma_z)$ are the radial, hoop, and axial stress components, respectively. Using the above defined dimensionless parameters, Eqs. (6) and (7) can be re-written as follow.

$$\left(1-\nu\right)\zeta\frac{\partial^2 U}{\partial R^2}+\left[\left(1-\nu\right)\frac{d\zeta}{dR}+\left(\frac{1-\nu}{R}-\frac{d\nu}{dR}\right)\zeta\right]\frac{\partial U}{\partial R}$$

$$+\left[\nu\frac{d\zeta}{dR}+\left(\frac{d\nu}{dR}-\frac{1-\nu}{R}\right)\zeta\right]\frac{U}{R} \tag{9}$$

$$-\frac{d\left[\left(1+\nu\right)\overline{\alpha}\zeta\right]}{dR}\theta-\left(1+\nu\right)\overline{\alpha}\zeta\frac{\partial\theta}{\partial R}=0$$

and

$$\overline{\sigma}_r\left(R_i,\tau\right) = -P_i \tag{10-a}$$

$$\overline{\sigma}_r\left(R_o,\tau\right) = -P_o \tag{10-b}$$

2.3 Solution of the Governing Equations Using Finite Difference Discretization

The governing equations (4) and (9) can be solved using a fully implicit finite difference method. This method has been previously used to solve the transient thermo-elasticity problems for solid cylinders made from FGMs (Darabseh & Salameh 2010) and for orthotropic homogeneous solid cylinders based on hyperbolic heat conduction model (Darabseh et al. 2008). The spatial derivatives of the temperature and the displacement at node j and time step $(k+1)$ are approximated using the central difference scheme, whereas the time derivative of the temperature at node i and time step $(k+1)$ is represented using the backward difference scheme. This is an unconditionally stable integration scheme with $O(\Delta R)^2$ accuracy for spatial derivatives and $O(\Delta\tau)$ for temporal derivative. The discretized finite difference form of Eq. (4) is given by

$$\begin{gathered}
\theta_{j+1}^{k+1}\left\{\overline{k}_j\left(\frac{2}{\Delta R}+\frac{1}{R_j}\right)+\left(\frac{d\overline{k}}{dR}\right)_{R=R_j}\right\}\frac{1}{2\Delta R}-\theta_j^{k+1}\left\{\frac{\overline{c}_j\overline{\rho}_j}{\Delta\tau}+\frac{2\overline{k}_j}{\left(\Delta R\right)^2}\right\} \\
\theta_{j-1}^{k+1}\left\{\overline{k}_j\left(\frac{2}{\Delta R}-\frac{1}{R_j}\right)-\left(\frac{d\overline{k}}{dR}\right)_{R=R_j}\right\}\frac{1}{2\Delta R}=-\theta_j^{k}\left\{\frac{\overline{c}_j\overline{\rho}_j}{\Delta\tau}\right\} \\
k=0,1,2,\ldots, \\
j=2,\ldots,N-1
\end{gathered} \tag{11}$$

where $R_j = R_i + (j-1)\,\Delta R$, $\tau_k = k\Delta\tau$, $\theta_j^k = \theta\left(R_j,\tau_k\right)$, $\overline{k}_j = \overline{k}\left(R_j\right)$, $\overline{\rho}_j = \overline{\rho}\left(R_j\right)$, and $\overline{c}_j = \overline{c}\left(R_j\right)$.

For the boundary nodes, i.e. $R = R_1 = R_i$ and $R = R_N = R_o$, the final finite difference scheme of the governing equations can be obtained by considering the finite difference form of the governing equation and the boundary conditions expressed in Eqs. (5-b) and (5-c). The final discretized finite difference form of the governing equation at the cylinder inner surface boundary node is given by.

$$\begin{gathered}
\theta_2^{k+1}\left\{\frac{2\overline{k}_1}{\left(\Delta R\right)^2}\right\}-\theta_1^{k+1}\left\{\frac{\overline{c}_1\overline{\rho}_1}{\Delta\tau}+\frac{2\overline{k}_1}{\left(\Delta R\right)^2}-H_i\left[\overline{k}_1\left(\frac{1}{R_i}-\frac{2}{\Delta R}\right)+\left(\frac{d\overline{k}}{dR}\right)_{R=R_i}\right]\right\} \\
=-\theta_1^{k}\left\{\frac{\overline{c}_1\overline{\rho}_1}{\Delta\tau}\right\}+H_i\theta_i\left\{\overline{k}_1\left(\frac{1}{R_i}-\frac{2}{\Delta R}\right)+\left(\frac{d\overline{k}}{dR}\right)_{R=R_i}\right\}
\end{gathered} \tag{12}$$

Similarly, the final discretized finite difference form of the governing equation at the cylinder outer surface boundary node is given by.

$$\theta_{N-1}^{k+1}\left\{\frac{2\overline{k}_N}{\left(\Delta R\right)^2}\right\}-\theta_N^{k+1}\left\{\frac{\overline{c}_N\overline{\rho}_N}{\Delta\tau}+\frac{2\overline{k}_N}{\left(\Delta R\right)^2}-H_o\left[\overline{k}_N\left(\frac{1}{R_o}+\frac{2}{\Delta R}\right)+\left(\frac{d\overline{k}}{dR}\right)_{R=R_o}\right]\right\}$$
$$=-\theta_N^k\left\{\frac{\overline{c}_N\overline{\rho}_N}{\Delta\tau}\right\}-H_o\theta_o\left\{\overline{k}_N\left(\frac{1}{R_o}+\frac{2}{\Delta R}\right)+\left(\frac{d\overline{k}}{dR}\right)_{R=R_o}\right\} \tag{13}$$

The initial condition is

$$\theta_j^0=0,\ \ j=1,2,\ldots,N \tag{14}$$

It is worth mentioning that the spatial derivative of any material parameter, for example the thermal conductivity, $d\overline{k}/dR$, in Eqs. (11)-(13), can be explicitly calculated or it can be approximated using the central finite difference scheme.

Similarly, the governing equations regarding the thermo-elastic deformation of the cylinder given in Eqs. (9) and (10) can be discretized using the finite difference method. The governing equation for the interior nodes at dimensionless time τ_{k+1} is given by

$$U_{j+1}\left\{\frac{\zeta_j}{\Delta R}\left[\left(1-\nu_j\right)\left(\frac{1}{\Delta R}+\frac{1}{2R_j}\right)-\frac{1}{2}\left(\frac{d\nu}{dR}\right)_{R=R_j}\right]+\frac{1-\nu_j}{2\Delta R}\left(\frac{d\zeta}{dR}\right)_{R=R_j}\right\}$$
$$-U_j\left\{\zeta_j\left[\left(1-\nu_j\right)\left(\frac{2}{\left(\Delta R\right)^2}+\frac{1}{R_j^2}\right)-\frac{1}{R_j}\left(\frac{d\nu}{dR}\right)_{R=R_j}\right]-\frac{\nu_j}{R_j}\left(\frac{d\zeta}{dR}\right)_{R=R_j}\right\}$$
$$U_{j-1}\left\{\frac{\zeta_j}{\Delta R}\left[\left(1-\nu_j\right)\left(\frac{1}{\Delta R}-\frac{1}{2R_j}\right)+\frac{1}{2}\left(\frac{d\nu}{dR}\right)_{R=R_j}\right]-\frac{1-\nu_j}{2\Delta R}\left(\frac{d\zeta}{dR}\right)_{R=R_j}\right\} \tag{15}$$
$$=\left(1+\nu_j\right)\overline{\alpha}_j\zeta_j\frac{\theta_{j+1}^{k+1}-\theta_{j-1}^{k+1}}{2\Delta R}+\left\{\frac{d\left[\left(1+\nu\right)\overline{\alpha}\zeta\right]}{dR}\right\}_{R=R_j}\theta_j^{k+1}$$
$$k=0,1,2,\ldots,$$
$$j=2,\ldots,N-1.$$

The displacement boundary condition at the inner surface boundary node can be written as

$$U_1\left\{-\frac{1}{R_i^2}+\frac{2}{\Delta R}\left(\frac{\nu_1}{R_i}-\frac{1-\nu_1}{\Delta R}\right)+\frac{1}{R_i\left(1-\nu_1\right)}\left(\frac{d\nu}{dR}\right)_{R=R_i}\right\}\zeta_1+U_2\left\{\frac{2\left(1-\nu_1\right)\zeta_1}{\left(\Delta R\right)^2}\right\}$$
$$=\frac{2\Delta R}{1-\nu_1}\left[\left(1+\nu_1\right)\overline{\alpha}_1\theta_1^{k+1}-\frac{P_i}{\zeta_1}\right] \tag{16}$$

$$\times\left\{\frac{\zeta_1}{\Delta R}\left[\left(1-\nu_1\right)\left(\frac{1}{\Delta R}-\frac{1}{2R_i}\right)+\frac{1}{2}\left(\frac{d\nu}{dR}\right)_{R=R_i}\right]-\frac{1-\nu_1}{2\Delta R}\left(\frac{d\zeta}{dR}\right)_{R=R_i}\right\}$$

$$+\left(1+\nu_1\right)\overline{\alpha}_1\zeta_1\frac{\theta_2^{k+1}-\theta_0^{k+1}}{2\Delta R}+\left\{\frac{d\left[\left(1+\nu\right)\overline{\alpha}\zeta\right]}{dR}\right\}_{R=R_i}\theta_1^{k+1}$$

Similarly, the displacement boundary condition at the outer surface boundary node can be written as

$$\begin{aligned}
&U_N\left\{-\frac{1}{R_o^2}-\frac{2}{\Delta R}\left(\frac{\nu_N}{R_o}+\frac{1-\nu_N}{\Delta R}\right)+\frac{1}{R_o\left(1-\nu_N\right)}\left(\frac{d\nu}{dR}\right)_{R=R_o}\right\}\zeta_N+U_{N-1}\left\{\frac{2\left(1-\nu_N\right)\zeta_N}{\left(\Delta R\right)^2}\right\}\\
&=\frac{2\Delta R}{1-\nu_N}\left[\frac{P_o}{\zeta_N}-\left(1+\nu_N\right)\overline{\alpha}_N\theta_N^{k+1}\right]\\
&\times\left\{\frac{\zeta_N}{\Delta R}\left[\left(1-\nu_N\right)\left(\frac{1}{\Delta R}+\frac{1}{2R_o}\right)-\frac{1}{2}\left(\frac{d\nu}{dR}\right)_{R=R_o}\right]+\frac{1-\nu_N}{2\Delta R}\left(\frac{d\zeta}{dR}\right)_{R=R_o}\right\}\\
&+\left(1+\nu_N\right)\overline{\alpha}_N\zeta_N\frac{\theta_{N+1}^{k+1}-\theta_{N-1}^{k+1}}{2\Delta R}+\left\{\frac{d\left[\left(1+\nu\right)\overline{\alpha}\zeta\right]}{dR}\right\}_{R=R_o}\theta_N^{k+1}
\end{aligned}\tag{17}$$

Note that because the inertia effects are neglected, it is possible to determine the nodal displacements independent of the displacement and the temperature history at the current time increment, i.e, by only using the temperature distribution in the FG cylinder at the current time increment. Also note that the right hand side of Eqs. (16) and (17) includes the terms θ_0^{k+1} and θ_{N+1}^{k+1}, respectively. These two virtual nodal temperatures can be obtained using the finite difference form of the thermal boundary conditions, i.e. Eqs. (5-b) and (5-c), which yields the followings

$$\theta_0^{k+1}=\theta_2^{k+1}+2H_i\Delta R\left(\theta_i-\theta_1^{k+1}\right)\tag{18-a}$$

$$\theta_{N+1}^{k+1}=\theta_{N-1}^{k+1}+2H_o\Delta R\left(\theta_o-\theta_N^{k+1}\right)\tag{18-b}$$

Equations (11) to (13) and (15) to (17), when written in matrix form, result in a tri-diagonal coefficients matrix, which allows use of the fast and efficient solution techniques for determination of the nodal values. Details of numerical techniques for the solution of problems with tri-diagonal coefficients matrix can be found for example in (Carnahan et al. 1969).

Once the distribution of the radial displacement in the cylinder is determined, the finite difference form of the radial and circumferential strains can be written as follow.

$$\left(\overline{\varepsilon}_r\right)_{R=R_j}=\frac{U_{j+1}-U_{j-1}}{2\Delta R}\tag{19-a}$$

$$\left(\overline{\varepsilon}_{\phi}\right)_{R=R_j} = \frac{U_j}{R_j} \qquad j = 1,2,\ldots,N \tag{19-b}$$

Similarly, the radial, circumferential, and axial stress components at each grid point at time step $(k+1)$ can be written as follow.

$$\left(\overline{\sigma}_r\right)_{R=R_j} = \zeta_j\left[\left(1-\nu_j\right)\left(\overline{\varepsilon}_r\right)_{R=R_j} + \nu_j\left(\overline{\varepsilon}_{\phi}\right)_{R=R_j}\right] - \left(1+\nu_j\right)\overline{\alpha}_j\zeta_j\theta_j^{k+1} \tag{20-a}$$

$$\left(\overline{\sigma}_{\phi}\right)_{R=R_j} = \zeta_j\left[\left(1-\nu_j\right)\left(\overline{\varepsilon}_{\phi}\right)_{R=R_j} + \nu_j\left(\overline{\varepsilon}_r\right)_{R=R_j}\right] - \left(1+\nu_j\right)\overline{\alpha}_j\zeta_j\theta_j^{k+1} \tag{20-b}$$

$$\left(\overline{\sigma}_z\right)_{R=R_j} = \nu_j\left[\left(\overline{\sigma}_r\right)_{R=R_j} + \left(\overline{\sigma}_{\phi}\right)_{R=R_j}\right] - \overline{E}_j\overline{\alpha}_j\theta_j^{k+1} \qquad j = 1,2,\ldots,N. \tag{20-c}$$

In Eq. (19-a) it is necessary to have the values of U_0 and U_{N+1} for the calculation of the radial strain component at the first and last spatial grid point, respectively. U_0 and U_{N+1} can be calculated using the finite difference form of the boundary conditions, given in Eqs. (10-a) and (10-b), respectively, as follow.

$$U_0 = U_2 - \frac{2\Delta R}{\left(1-\nu_1\right)}\left[\left(1+\nu_1\right)\overline{\alpha}_1\theta_1^{k+1} - \frac{\nu_1 U_1}{R_i} - \frac{P_i}{\zeta_1}\right] \tag{21-a}$$

$$U_{N+1} = U_{N-1} + \frac{2\Delta R}{\left(1-\nu_N\right)}\left[\left(1+\nu_N\right)\overline{\alpha}_N\theta_N^{k+1} - \frac{\nu_N U_N}{R_o} - \frac{P_o}{\zeta_N}\right] \tag{21-b}$$

3 STRESS INTENSITY FACTOR CALCULATION USING THE WEIGHT FUNCTION METHOD

In the previous section, stress distribution in the un-cracked FG cylinder was numerically calculated. The weight function method requires this stress distribution for the calculation of SIF values. In this section, the weight function method is used to calculate the transient thermal SIF of FG cylinders.

First, we consider an internally pressurized cylinder with an internal circumferential crack. For this case, the time-dependent dimensionless mode-I thermal SIF, corresponding to the dimensionless normal stress distribution along the crack face in the un-cracked body $\overline{\sigma}_z\left(R,\tau\right)$, can be calculated using the following integral equation.

$$\overline{K}_I\left(\tau\right) = \int_{R_i}^{R_i+\overline{a}}\left[\overline{\sigma}_z\left(R,\tau\right) + P_i\right]\Psi\left(R,\overline{a}\right)dR \tag{22}$$

where $\overline{K}_I\left(\tau\right) = K_I\left(\tau\right)\Big/\left(E_{ref}\alpha_{ref}T_{ef}\sqrt{r_{ref}}\right)$, with $K_I\left(\tau\right)$ being the mode-I SIF, and $\overline{a} = a\big/r_{ref}$ representing the dimensionless crack depth. The dimensionless form of the weight function for a hollow cylinder with internal circumferential crack $\Psi\left(R,\overline{a}\right)$ is given by (Glinka & Shen 1991)

$$\Psi\left(R,\overline{a}\right)=\sqrt{\frac{2}{\pi\left(\overline{a}-\overline{y}\right)}}\left[1+M_1\left(1-\frac{\overline{y}}{\overline{a}}\right)^{1/2}+M_2\left(1-\frac{\overline{y}}{\overline{a}}\right)+M_3\left(1-\frac{\overline{y}}{\overline{a}}\right)^{3/2}\right] \tag{23}$$

Where $\overline{y}=R-R_i$. In Eq. (23) three unknown coefficients M_j (j=1, 2, 3) exist which can be determined using reference SIFs, $\overline{K}_r$, corresponding to three reference load cases applied to the crack faces (reference stresses). Reference SIFs can be determined using any analytical and/or numerical method including the FE method. By substituting Eq. (23) and the reference SIFs, $\overline{K}_r$, into Eq. (22), the unknown coefficients of the weight function can be calculated. Jones and Rothwell (Jones & Rothwell 2001) have suggested use of the uniform, linear, and quadratic surface pressure loads as the reference stresses (load cases) for obtaining the reference SIF values. These three reference load cases are considered in this work and are defined as follow.

Reference load Case (1) – uniform distribution $\quad \overline{\sigma}\left(R\right)=\overline{\sigma}_0$ (24-a)

Reference Load Case (2) – linear distribution $\quad \overline{\sigma}\left(R\right)=\overline{\sigma}_0\left(\frac{R-R_i}{R_o-R_i}\right)$ (24-b)

Reference Load Case (3) – quadratic distribution $\quad \overline{\sigma}\left(R\right)=\overline{\sigma}_0\left(\frac{R-R_i}{R_o-R_i}\right)^2$ (24-c)

where $\overline{\sigma}_0$ is the dimensionless uniform applied stress. Dimensionless reference SIFs for the above three reference load cases, also known as the boundary correction factors, are defined as $Y_j=\overline{K}_{rj}\big/\overline{\sigma}_0\sqrt{\pi\overline{a}}$ (j=1, 2 ,3). With the help of the boundary correction factors Y_j, coefficients M_j in Eq. (23) can be determined as follow (Jones & Rothwell 2001)

$$M_1=-\frac{48}{5}+\pi\sqrt{2}\left[6Y_1-39\left(\frac{\overline{a}}{R_o-R_i}\right)^{-1}Y_2+42\left(\frac{\overline{a}}{R_o-R_i}\right)^{-2}Y_3\right] \tag{25-a}$$

$$M_2=21-\pi\sqrt{2}\left[\frac{105}{4}Y_1-\frac{315}{2}\left(\frac{\overline{a}}{R_o-R_i}\right)^{-1}Y_2+\frac{315}{2}\left(\frac{\overline{a}}{R_o-R_i}\right)^{-2}Y_3\right] \tag{25-b}$$

$$M_2=-\frac{64}{5}+\pi\sqrt{2}\left[24Y_1-132\left(\frac{\overline{a}}{R_o-R_i}\right)^{-1}Y_2+126\left(\frac{\overline{a}}{R_o-R_i}\right)^{-2}Y_3\right] \tag{25-c}$$

In what follows, the transient thermal stress distribution, which was numerically integrated in the previous section, is substituted in Eq. (22) and Eq. (22) is numerically integrated to obtain the

transient SIF values. MATLAB® "*integral*" built-in function (MathWorks Inc. 2013) is used for numerical integration. This function can handle the singularity that exists in the weight function expression.

4 FE ANALYSIS FOR STRESS INTENSITY FACTOR CALCULATION OF THE FG CYLINDER

As discussed in section 3, determination of the weight function coefficients requires knowledge of three reference SIFs. The reference SIFs can be calculated for the uniform, linear, and quadratic crack face pressure loads given in Eq. (24) using the FE analysis. In this section, FE modeling and post-processing step for the calculation of reference SIFs are described.

Once the weight function coefficients are determined, the developed combined finite difference-weight function technique is used for the prediction of transient thermomechanical SIFs. To validate and assess the accuracy of the proposed weight function results, additional FE analyses have been done to calculate transient thermal SIFs corresponding to thermomechanical loads. The predicted SIFs from the weight function method are compared to the obtained FE SIF results.

4.1 Finite Element Modeling

The infinitely long FG hollow cylinder, shown in Fig. 1, with inner and outer radii r_i and r_o, and a complete internal circumferential crack of depth a, was considered in all of the FE modeling cases. ABAQUS Standard commercial software (Simulia, Dassault Systèmes. 2012) was used for the FE model generation. The cylinder thermal and mechanical properties gradation were implemented in the FE model using ABAQUS user subroutines UMATHT and UMAT, respectively. These two subroutines assign the corresponding generic property values to each integration point of each element. Furthermore, the process of FE model crack generation and analysis for different crack depth to cylinder wall thickness ratios and different FG gradation profiles was automated by developing an ABAQUS Python script. ABAQUS quadratic axisymmetric elements DCAX8 for the transient heat transfer analysis and quadratic axisymmetric elements CAX8 for the static analysis with full integration option were used in all of the FE analyses. Due to the reflective symmetry property of the longitudinal section of the cylinder, half of the cylinder longitudinal section was modeled in all FE analyses. To have the plane strain condition, the far end of the cylinder was fixed toward the axial direction in all FE models. Mesh convergence studies suggested that the element size in the first five contour regions around the crack tip should not exceed 1 percent of the crack depth. Temperature distribution results from the transient heat transfer FE analysis were used as predefined temperature field in the form of body loads in the FE static analysis.

4.2 *J*-Integral for FG Cylinders with Circumferential Cracks

To calculate the SIF values from the FE analysis results, a domain form of the *J*-integral expression for FG cylinders with a complete internal circumferential crack is used here.

The axisymmetric domain form of the *J*-integral expression for FG cylinders with a complete internal circumferential crack is given by (Eshraghi & Soltani 2015a; Shih et al. 1986)

$$J = \frac{1}{r_{\text{tip}}}\left\{\int_A \left[\sigma_{\eta\gamma}\frac{\partial u_\eta}{\partial r}\frac{\partial q}{\partial \gamma} - W\left(\frac{\partial q}{\partial r}+\frac{q}{r}\right)+\left(\frac{u_r}{r^2}\sigma_{\phi\phi} - \left.\frac{\partial W}{\partial r}\right|_{\text{expl}}\right)q\right] rdA \right.$$
$$\left. + \int_{S^U - S^L}\frac{\partial u_z}{\partial r}\sigma_{zz} q r dS\right\} \tag{26}$$

where subscripts η and γ range over the radial r and the axial z directions, respectively. $u = \left(u_r, 0, u_z\right)$ denotes the displacement field, $\left(\sigma_{rr}, \sigma_{\phi\phi}, \sigma_{zz}\right)$ are the normal components of the stress tensor and σ_{rz} is the transverse shear stress in the cracked FG cylinder. r_{tip} is the radius of the crack front with respect to the longitudinal axis of the cylinder, and A is the domain of integration ahead of the crack tip. Parameter q is a function that varies smoothly from unity on the crack front to zero on the boundary of the domain A. In Eq. (26), S^U and S^L denote the top and the bottom crack faces located in the integration domain, respectively, and W is the strain energy density corresponding to the applied thermomechanical loads. The term $\left.\frac{\partial W}{\partial r}\right|_{\text{expl}}$ in Eq. (26), is the explicit derivative of the strain energy density with respect to the r coordinate by retaining the strain terms as constant in the energy density expression. It is defined by

$$\left.\frac{\partial W}{\partial r}\right|_{\text{expl}} = \frac{\partial W}{\partial E}\frac{dE}{dr} + \frac{\partial W}{\partial \alpha}\frac{d\alpha}{dr} + \frac{\partial W}{\partial T}\frac{\partial T}{\partial r} \tag{27}$$

The reader is referred to (Eshraghi & Soltani 2015a) for more details regarding the axisymmetric J-integral for FG cylinders. Also, details on the numerical implementation of the J-integral can be found in (Anlas et al. 2000; Dag 2006).

Once the J-integral value is obtained, the mode-I SIF can be calculated as follows

$$K_I = \sqrt{JE_{\text{tip}}\Big/\left(1-\nu_{\text{tip}}^2\right)} \tag{28}$$

where E_{tip} and ν_{tip} are the elastic modulus and the Poisson's ratio values at the crack tip location, respectively.

5 RESULTS

In this section, transient thermal SIF results obtained from both the direct FE analysis and the finite difference-weight function technique are presented and compared to each other. Presented results are for a hollow FG cylinder with its outer radius being twice its inner radius, i.e. $R_o = 2R_i$. Thermal and mechanical properties (except the Poisson's ratio) of the FG cylinder vary through the cylinder wall thickness according to the following equation.

$$\overline{\Upsilon} = R^\lambda \tag{29}$$

where λ is the FGM power law index and represents the variation of the cylinder material properties along the cylinder wall thickness. $\overline{\Upsilon}$ is a normalized generic material property defined as the ratio of its value to the corresponding material property value at the inner surface of the cylinder. It should be noted that all reference values are set to those of the cylinder inner radius and the reference temperature is set to unity in this work. The Poisson's ratio is assumed to be constant everywhere with value 0.3. Note that for a homogeneous cylinder $\lambda = 0$ and all material properties are constant and identical to the material property value at the inner surface of the cylinder, i.e. $\overline{\Upsilon} = 1$. It is assumed that the FG cylinder is subjected to internal convection cooling and internal pressure whereas the fluid around the cylinder outer surface has temperature equal to the initial temperature of the cylinder. The following numerical values are used for the dimensionless thermal and mechanical boundary conditions.

$$\theta_i = -1,\ \theta_o = 0,\ \overline{h}_i = 50,\ \overline{h}_o = 5,$$

$$P_i = 1,\ P_o = 0.$$

To assess the accuracy of obtained temperature and stress distribution for the FG cylinder discussed above, the steady state temperature distribution and stress components across the cylinder wall thickness obtained from the finite difference (FD) and finite element (FE) analyses are compared to each other and are shown in Figs. 2-4. Also, analytical solutions given in (Jabbari et al. 2002) are plotted in these figures. Very good agreement is observed between the results of the present analysis based on the FD analyses with both the FE and the exact analytical results.

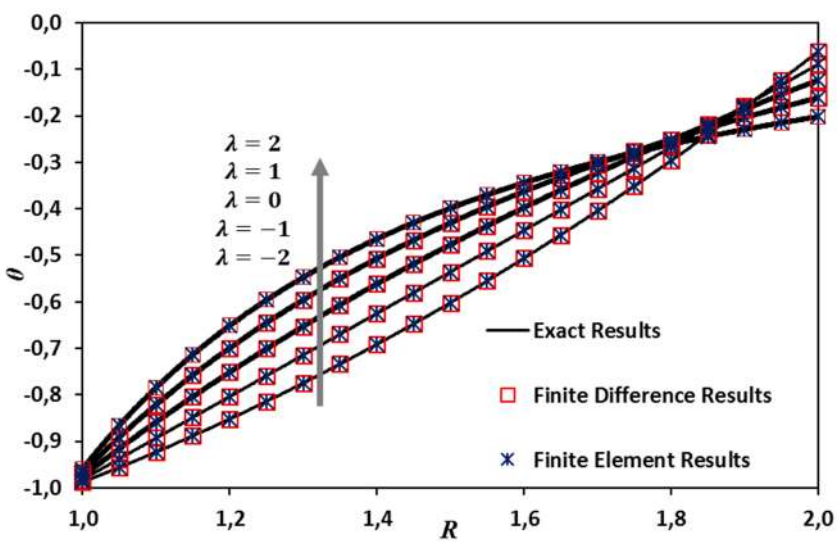

Figure 2: Comparison of dimensionless steady state temperature distribution in FG cylinders for different FG power law indices.

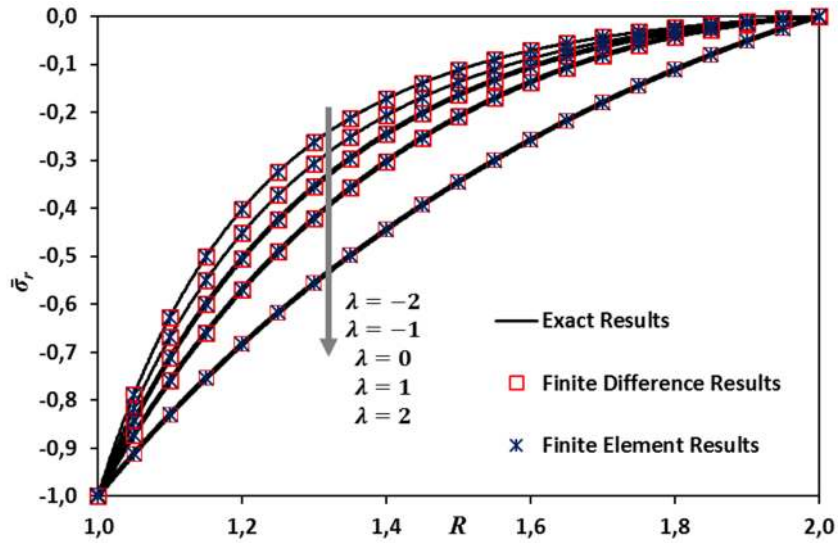

Figure 3: Comparison of dimensionless steady state radial stress distribution in FG cylinders for different FG power law indices.

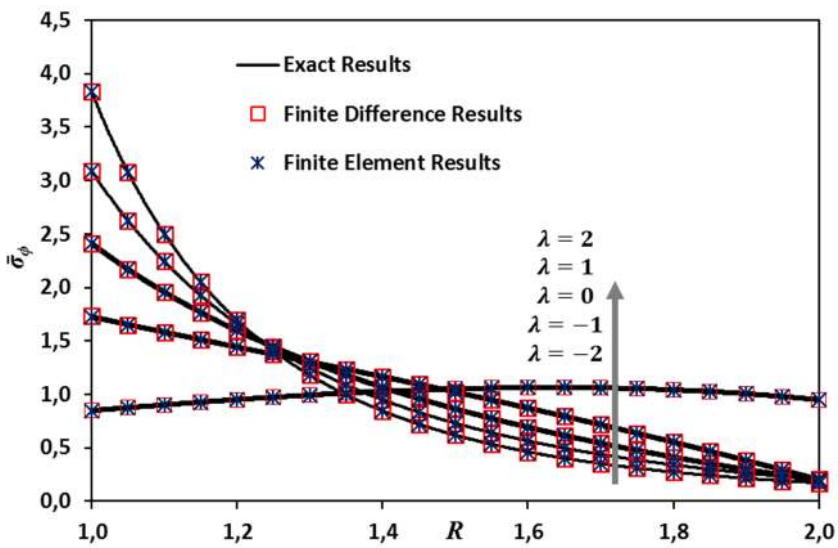

Figure 4: Comparison of dimensionless steady state circumferential stress distribution in FG cylinders for different FG power law indices.

The presented FD and FE approaches can now be used to obtain transient thermomechanical SIFs for the FG cylinder. To determine the SIFs using the FD method combined with the weight function approach, we need to know the values of the boundary correction factors, Y_j. Based on the results of the FE analysis conducted in this study, the following expression may be used to predict the boundary correction factors of the FG cylinder considered in this work.

$$Y_j = \left(A_{j0} + \exp \sum_{k=1}^{7} A_{jk} \beta^{k-1} \right) \left(1 + \sum_{m=1}^{3} \sum_{n=0}^{m} A_{js} \beta^n \lambda^{m-n} \right)$$
$$s = \frac{\left(m-1\right)\left(m+2\right)}{2} + n + 8 \tag{30}$$

where $\beta = \overline{a} \big/ \left(R_o - R_i \right)$ is the crack depth ratio, and λ is the FG power law index. The unknown coefficients in Eq. (30), i.e. $A_{jl} \left(j = 1,2,3;\ l = 0,1,\ldots,16 \right)$, can be determined with the help of a non-linear least squares scheme using the extracted FE results. The calculated values for these coefficients are listed in Table 1.

Fitting coefficient	j=1	j=2	j=3
A_{j0}	0.6506	-0.8814	-0.01658
A_{j1}	-0.7087	-0.1022	-4.109
A_{j2}	4.578	0.2016	-0.9491
A_{j3}	5.948	6.781	59.48
A_{j4}	-32.56	-20.21	-181.3
A_{j5}	75.48	55.9	283.5
A_{j6}	-82.88	-70.26	-227.9
A_{j7}	34.6	30.88	73.65
A_{j8}	-0.02175	-0.01335	-0.01076
A_{j9}	-2.906	-2.828	-2.36
A_{j10}	3.238×10^{-4}	6.181×10^{-5}	3.992×10^{-5}
A_{j11}	0.05498	0.03026	0.02237
A_{j12}	3.187	3.024	1.996
A_{j13}	-1.088×10^{-6}	-7.324×10^{-8}	1.731×10^{-6}
A_{j14}	-9.214×10^{-5}	2.572×10^{-4}	2.921×10^{-4}
A_{j15}	-0.03231	-0.01491	-9.392×10^{-3}
A_{j16}	-1.242	-1.102	-0.4949

Table 1: Curve fitting function coefficients for the three boundary correction factors.

Results of transient thermomechanical SIFs for cylinders with $\lambda = -2, 0, 2$ with dimensionless time are presented in Figs. 5-7. It is worth mentioning that in what follows the calculated SIFs are presented in the following normalized form.

$$\bar{K}_I^N \left(\tau \right) = \bar{K}_I \left(\tau \right) \big/ P_i \sqrt{\pi \overline{a}} \tag{31}$$

From Figs. 5-7, the SIF values increase with time until they reach to their steady state values. Note that SIFs at $\tau = 0$ correspond to the case for which the cylinder is subjected to internal pressure only. From Fig. 5 it is observed that for a FG cylinder with $\lambda = -2$, a 10% wall thickness shallow crack, $\beta = 0.1$, can have SIF values comparable in magnitude to those of a 90% wall thickness deep crack, $\beta = 0.9$. Also a 20% wall thickness crack depth, $\beta = 0.2$, shows higher transient SIFs compared to those of the crack depths with ratios $\beta \leq 0.8$. This is in contrast to the case of $\tau = 0$, i.e.

internal pressure loading only, where the SIF values increase with increasing crack depth ratio. This suggests that the thermal boundary conditions can influence the SIF values of a FG cylinder with $\lambda = -2$ and with shallow cracks. This effect is considerably smaller for deep cracks.

For a homogeneous cylinder with $\lambda = 0$, Fig. 6 shows that the SIFs are close to each other for shallow cracks whereas for deep cracks the SIFs are relatively higher. Also, from Figs. 5 and 6, it is observed that for the homogenous cylinder the transition time required to reach the steady state is more than twice the transition time required for the FG cylinders with $\lambda = -2$. From Fig. 7, for the case of $\lambda = 2$ and small magnitudes of dimensionless time, shallow cracks have higher transient SIFs compared to those of the medium crack depth ratios. The steady state SIFs monotonically increase with increasing crack depth.

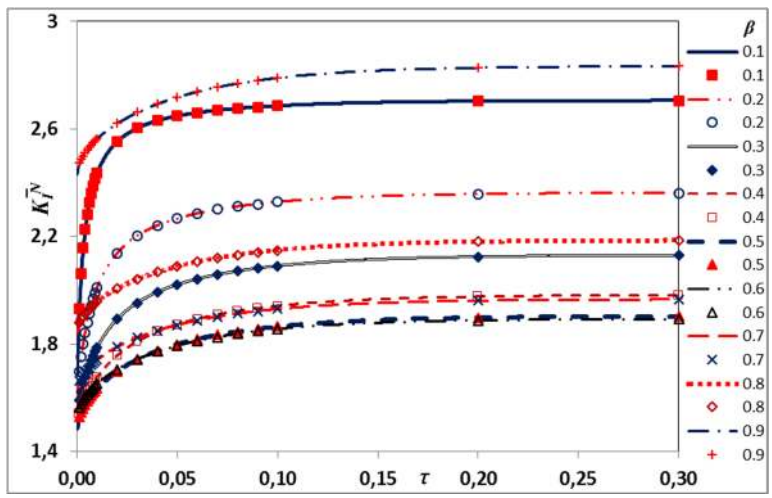

Figure 5: Time history of normalized SIF for different crack depth ratios of a FG cylinder with λ = –2; lines: finite difference (FD) results, symbols: finite element (FE) results.

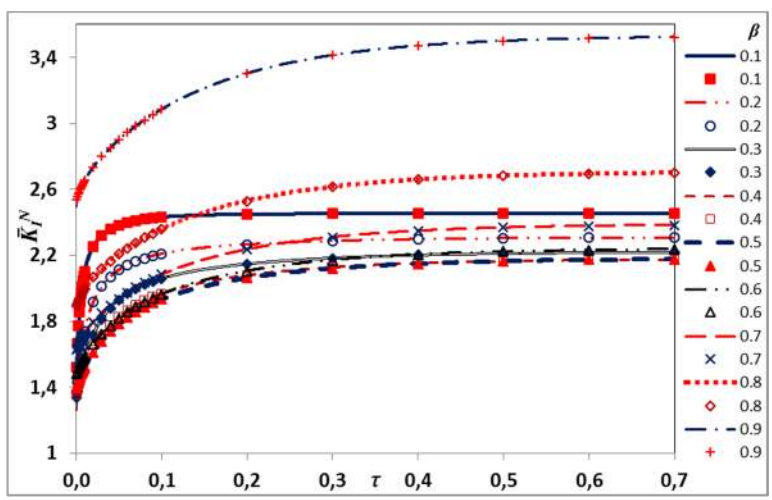

Figure 6: Time histories of normalized SIF for different crack depth ratios of a FG cylinder with λ = 0; lines: finite difference results, symbols: finite element results.

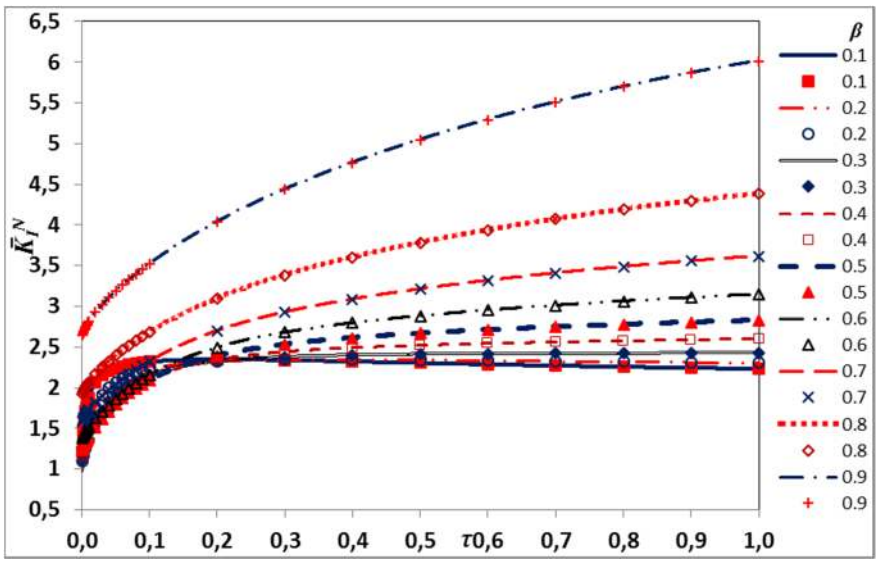

Figure 7: Time histories of normalized SIF for different crack depth ratios of a FG cylinder with $\lambda = 2$; lines: finite difference results, symbols: finite element results.

From Figs. 5-7 it can be concluded that the transient thermomechanical SIFs greatly depend on the crack depth ratio at small magnitudes of dimensionless time. Also, the power law index has a considerable effect on the SIF values for deep cracks. For example, by comparing Fig. 7 to Fig. 5 it can be observed that the steady state response of a FG cylinder with $\beta = 0.9$ and $\lambda = 2$ shows SIF values more than twice greater than those of a cylinder with $\lambda = -2$.

Figs. 8-11 show the transient thermomechanical SIFs for FG cylinders with $\lambda = -4, -1, 1, 4$ for different dimensionless time values. Fig. 8 indicates that for the FG power law index $\lambda = -4$, SIFs monotonically increase with increasing time for all values of crack depth ratios. Results presented in Fig. 8 also show that for shallow cracks SIF values increase over time at higher rate than deep cracks. Almost for all of the time scale values shown in Fig. 8, FG cylinders with crack depth ratio $\beta = 0.1$ have the highest SIF values. At $\tau = 0.1$, the SIF values have already reached their steady state condition for all crack depth ratios. For the FG cylinders with $\lambda = -1$, Fig. 9 indicates that the time required for SIFs to reach their steady state values has increased to $\tau = 0.5$, as compared to the case of $\lambda = -4$. In this case, deep cracks with $\beta = 0.9$ have largest SIF values for all time scale magnitudes. Note that the lowest SIFs occur for the FG cylinders with crack depth ratios in the range of $0.4 \le \beta \le 0.6$ for negative power law index values.

Fig. 10 shows the variation of SIFs at different times for the FG cylinders with power law index $\lambda = 1$. It is observed that deep cracks with $\beta = 0.9$ have the highest SIFs at all of the time values. Also, compared to FG cylinders with shallow cracks, it takes longer for deeply cracked cylinders to reach their steady state SIFs. For the case of FG cylinders with power law index $\lambda = 4$ and deep cracks, as Fig. 11 shows, the variation of SIFs over time is much higher than those of shallow cracks. It is also observed that the steady state SIF values are lower than their initial values for shallow

cracks whereas for deep cracks the steady state SIF values are more than ten times greater than their initial values. The time required to attain steady state conditions are also relatively longer for the FG cylinders with $\lambda = 4$.

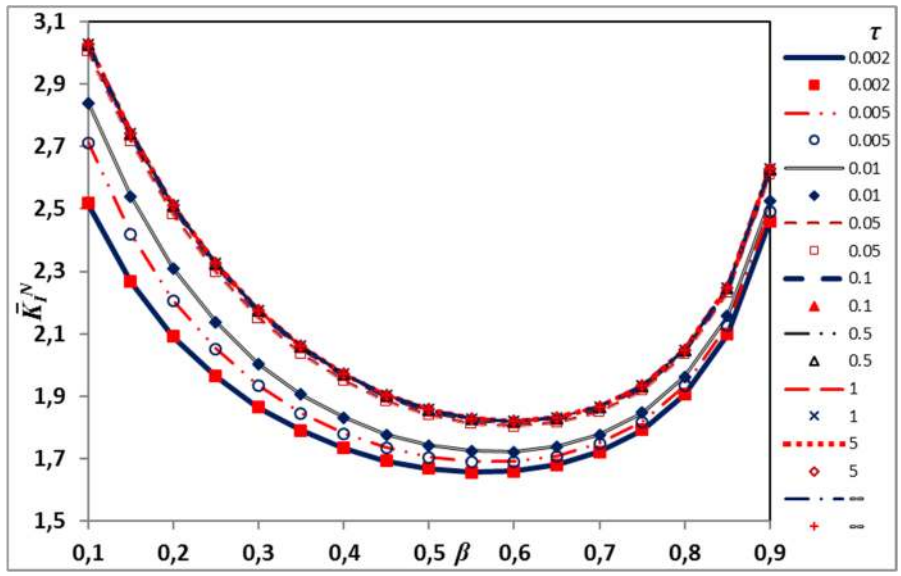

Figure 8: Variation of normalized SIF with crack depth ratio for a FG cylinder with $\lambda = -4$ at different dimensionless time values; lines: finite difference results, symbols: finite element results.

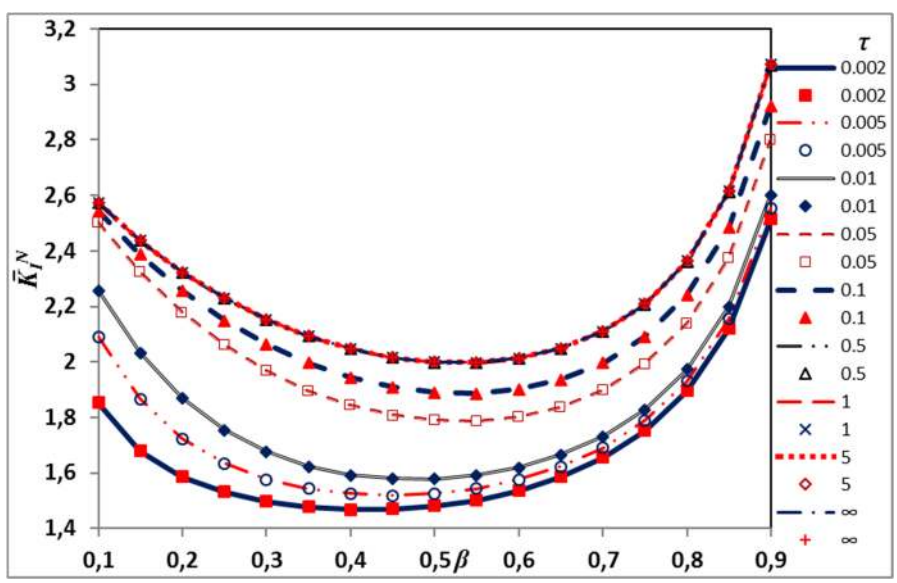

Figure 9: Variation of normalized SIF with crack depth ratio for a FG cylinder with $\lambda = -1$ at different dimensionless time values; lines: finite difference results, symbols: finite element results.

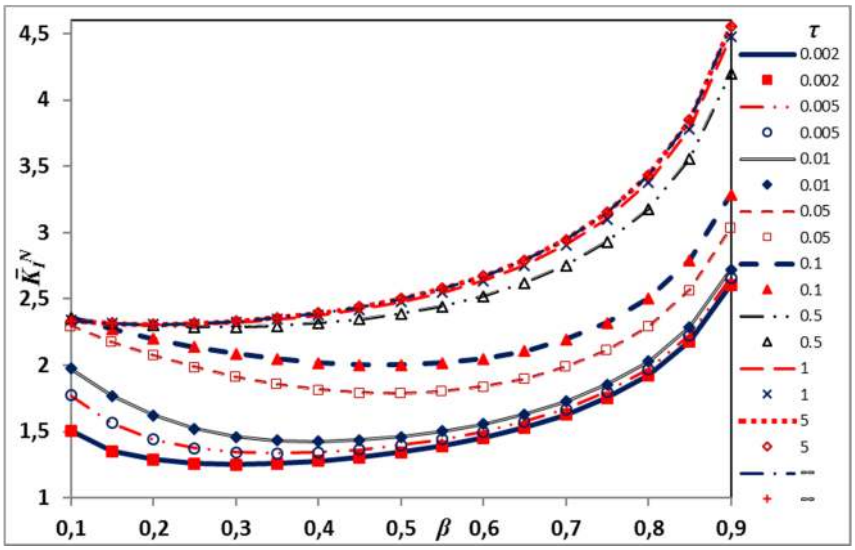

Figure 10: Variation of normalized SIF with crack depth ratio for a FG cylinder with $\lambda = 1$ at different dimensionless time values; lines: finite difference results, symbols: finite element results.

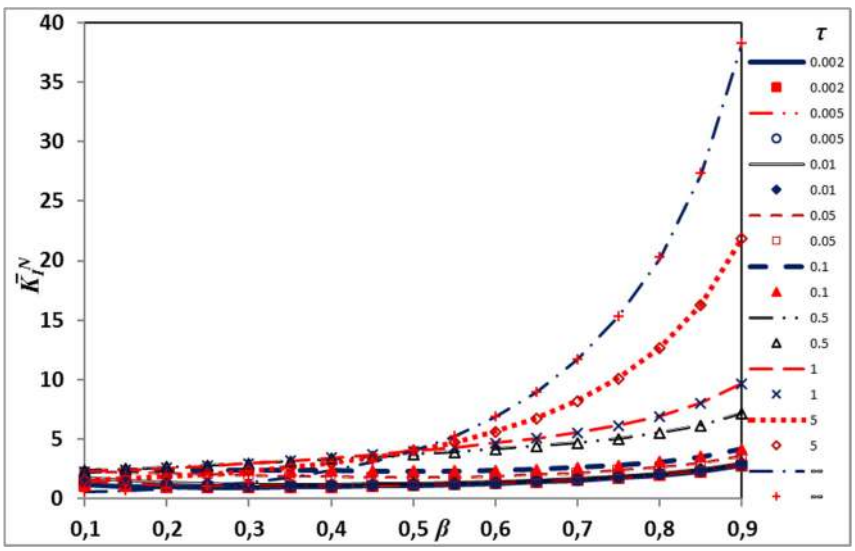

Figure 11: Variation of normalized SIF with crack depth ratio for a FG cylinder with $\lambda = 4$ at different dimensionless time values; lines: finite difference results, symbols: finite element results.

Thermomechanical SIF results for different FG power law indexes at fixed dimensionless time value $\tau = 0.001$ are shown in Fig. 12. From this figure, for the crack depth ratios $\beta < 0.7$, SIFs decrease with increasing λ whereas for deep cracks SIFs increase with increasing λ. It is observed that for deep cracks and at small time values, the FG power law index has small effect on the SIF values. A similar trend is observed for the dimensionless time value $\tau = 0.02$ as shown in Fig. 13. It is also observed that for negative λ, SIFs of shallow cracks are higher or equal to SIFs of deeply cracked cylinders. As shown in Fig. 14, at time $\tau = 0.2$ the influence of the FG power law index on the SIF

values are highest for deeply cracked cylinders. From this figure, SIFs monotonically increase with the crack depth for FG cylinders with $\lambda \geq 3$. On the other hand, the crack depth ratio has less effect on the SIF values for FG cylinders with negative λ and for homogeneous cylinders. Fig. 15 shows the steady state SIFs for the FG cylinders. From this figure one can observe that the crack depth ratio has small effect on the steady state thermomechanical SIF values for FG cylinders with $\lambda \leq 0$, whereas for FG cylinders with positive power law index deeply cracked cylinders have high SIF values compared to the cylinders with shallow cracks. In addition, for shallow cracks, FG cylinders with positive λ value have smaller SIFs compared to cracked FG cylinders with $\lambda \leq 0$.

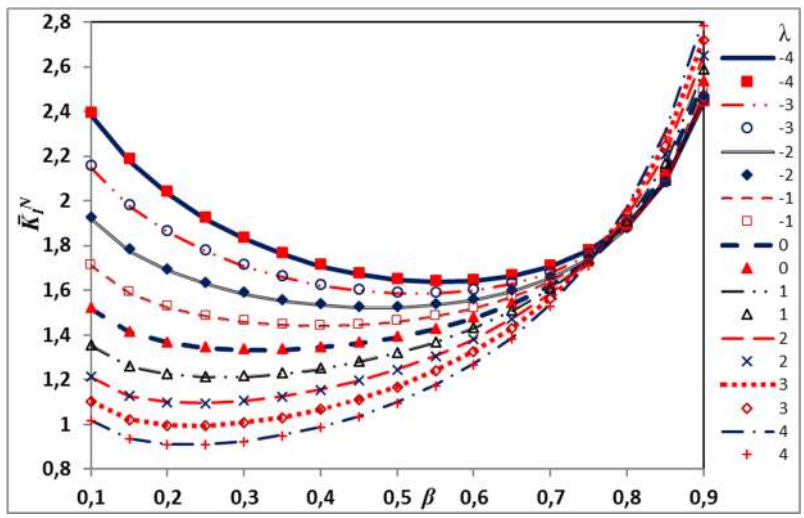

Figure 12: Variation of normalized SIF with crack depth ratio for FG cylinders with different power law indices at $\tau = 0.001$; lines: finite difference results, symbols: finite element results.

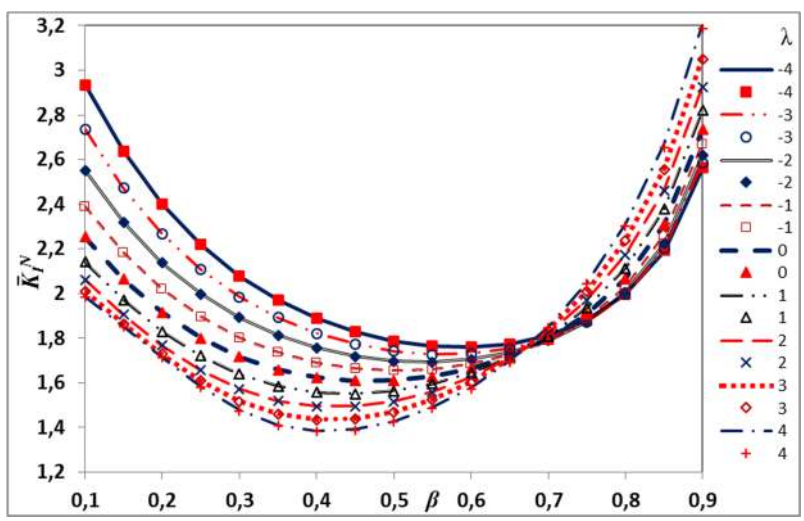

Figure 13: Variation of normalized SIF with crack depth ratio for FG cylinders with different power law indices at $\tau = 0.02$; lines: finite difference results, symbols: finite element results.

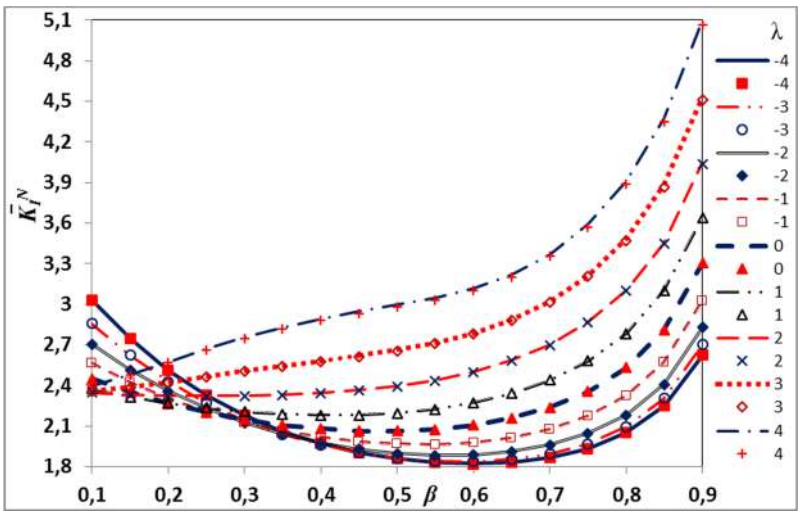

Figure 14: Variation of normalized SIF with crack depth ratio for FG cylinders with different power law indices at $\tau = 0.2$; lines: finite difference results, symbols: finite element results.

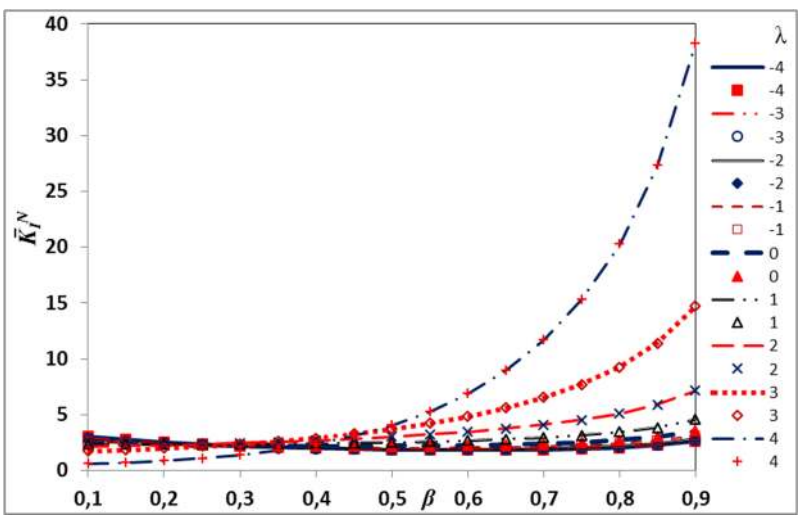

Figure 15: Variation of normalized SIF with crack depth ratio for FG cylinders with different power law indices at steady state conditions; lines: finite difference results, symbols: finite element results.

6 CONCLUSIONS

In this work, the weight function method was used to determine transient thermomechanical SIFs of infinitely long hollow FG cylinders with internal circumferential cracks. The finite difference method was used to compute the temperature and the stress distribution in the cylinder. The finite difference integration technique resulted in tri-diagonal coefficient matrices which allowed use of computationally efficient algorithms for obtaining the numerical solutions. Furthermore, FE analysis was performed to determine unknown coefficients of the weight function expression as well as to investigate the accuracy of the predicted transient thermomechanical SIFs by the presented weight function

method. The proposed method of combined finite difference technique and the weight function method for the determination of SIFs can be used for arbitrary variation of material properties. This is because no particular material gradation profile was prescribed when integrating the governing equations.

Numerical results for transient SIFs were presented for FG cylinders with a power law gradation profile. The effects of the crack depth, the FGM power law index, and the time on the thermomechanical SIFs were investigated in detail. It was shown that transient thermal loads can result in significant variation in the SIF values during the transition period. For the loading conditions considered in this work, SIFs monotonically increase with increasing time for all crack depth ratios with negative material power law index values. The transient SIFs were higher than their steady state values for FG cylinders with shallow cracks and with positive FG power law indices. It was also shown that shallow cracks have SIFs comparable in magnitude to those of the deep cracks when transient thermal loads are present. The required time for the SIFs to attain their steady values was considerably higher for increasing power law index values. In the beginning and in the middle of the transition period, SIFs of FG cylinders with shallow cracks decrease with increasing FG power law index. For deeply cracked cylinders with higher power law index values, SIFs were higher in magnitude, as well. For all cases considered in this study, very good agreement was observed between the FE analysis results and the weight function results.

The technique proposed in the current study is accurate and fast and can be used for the determination of SIFs in FG cylinders subjected to thermomechanical loads. The presented technique is general and can be applied to any arbitrary material gradation profile. The presented technique can be used for the determination of optimized material gradation profile in order to obtain a desired fracture characteristic for the FG cylinder.

Acknowledgements

Support from the Iran National Science Foundation (INSF) is gratefully acknowledged. The authors would like to thank Dr. Mohammad Amin Eshraghi for his helpful comments by reading the draft of the manuscript.

References

Afsar, A.M., Anisuzzaman, M., Song, J.I. (2009). Inverse problem of material distribution for desired fracture characteristics in a thick-walled functionally graded material cylinder with two diametrically-opposed edge cracks, Engineering Fracture Mechanics 76: 845–855.

Afsar, A.M., Anisuzzaman, M. (2007). Stress intensity factors of two diametrically opposed edge cracks in a thick-walled functionally graded material cylinder, Engineering Fracture Mechanics 74: 1617–1636.

Afzal, M. A. F., Kesarwani, P., Reddy, K. M., Kalmodia, S., Basu, B., Balani, K. (2012). Functionally graded hydroxyapatite-alumina-zirconia biocomposite: Synergy of toughness and biocompatibility, Materials Science and Engineering: C 32: 1164–1173.

Ando, M., Hasebe, S., Kobayashi, S., Kasahara, N., Toyoshi, A., Ohmae, T., Enuma, Y. (2013). Thermal transient test and strength evaluation of a thick cylinder model made of Mod.9Cr-1Mo steel, Nuclear Engineering and Design 255: 296–309.

Anlas, G., Santare, M. H., Lambros, J. (2000). Numerical calculation of stress intensity factors in functionally graded materials, International Journal of Fracture 104: 131–143.

Bahr, H-A., Balke, H., Fett, T., Hofinger, I., Kirchhoff, G., Munz, D., Neubrand, A., Semenov, A. S., Weiss, H-J., Yang, Y. Y. (2003). Cracks in functionally graded materials, Materials Science and Engineering: A 362: 2–16.

Baig, M. N., Khalid, F. A., Khan, F. N., Rehman, K. (2014). Properties and residual stress distribution of plasma sprayed magnesia stabilized zirconia thermal barrier coatings, Ceramics International 40: 4853–4868.

Bayesteh, H., Mohammadi, S. (2013). XFEM fracture analysis of orthotropic functionally graded materials, Composites Part B: Engineering 44: 8–25.

Carnahan, B., Luther, H.A., Wilkes, J.O. (1969). Applied numerical methods, Wiley (New York).

Dag, S. (2006). Thermal fracture analysis of orthotropic functionally graded materials using an equivalent domain integral approach, Engineering Fracture Mechanics 73: 2802–2828.

Darabseh, T., Naji, M., Al-Nimr, M. (2008). Transient thermal stresses in an orthotropic cylinder under the hyperbolic heat conduction model, Heat Transfer Engineering 29: 632–642.

Darabseh, T., Salameh, K.B. (2010). Numerical solution of transient thermal stresses in a functionally graded cylinder. In 3rd WSEAS international conference on engineering mechanics, structures, engineering geology. 89–96.

Eshraghi, I., Dag, S., Soltani, N. (2015). Consideration of spatial variation of the length scale parameter in static and dynamic analyses of functionally graded annular and circular micro-plates, Composites Part B: Engineering 78: 338–348.

Eshraghi, I., Soltani, N. (2015a). Stress intensity factor calculation for internal circumferential cracks in functionally graded cylinders using the weight function approach, Engineering Fracture Mechanics 134: 1–19.

Eshraghi, I., Soltani, N. (2015b). Thermal stress intensity factor expressions for functionally graded cylinders with internal circumferential cracks using the weight function method. Theoretical and Applied Fracture Mechanics 80: 170–181.

Fett, T. (1992). Direct determination of weight functions from reference loading cases and geometrical conditions, Engineering Fracture Mechanics 42: 435–444.

Fett, T., Munz, D., Yang, Y.Y. (2000a). Direct adjustment procedure for weight functions of graded materials, Fatigue and Fracture of Engineering Materials and Structures 23: 191–198.

Fett, T., Munz, D., Yang, Y.Y. (2000b). Applicability of the extended Petroski–Achenbach weight function procedure to graded materials, Engineering Fracture Mechanics 65: 393–403.

Garcia, J., Pitonak, R. (2013). The role of cemented carbide functionally graded outer-layers on the wear performance of coated cutting tools, International Journal of Refractory Metals and Hard Materials 36: 52–59.

Ghajar, R., Nabavi, S.M. (2010). Closed-form thermal stress intensity factors for an internal circumferential crack in a thick-walled cylinder, Fatigue & Fracture of Engineering Materials & Structures 33: 504–512.

Gharooni, H., Ghannad, M., Zamani Nejad, M. (2016). Thermo-elastic analysis of clamped-clamped thick FGM cylinders by using third-order shear deformation theory, Latin American Journal of Solids and Structures, an ABCM Journal 13: 750–774.

Glinka, G., Shen, G. (1991). Universal features of weight functions for cracks in mode I, Engineering Fracture Mechanics 40: 1135–1146.

Grebner, H. (1985). Finite element calculation of stress intensity factors for complete circumferential surface cracks at the outer wall of a pipe, International Journal of Fracture 27: R99–R102.

Guo, L., Noda, N., (2014). Investigation methods for thermal shock crack problems of functionally graded materials–part I: analytical method, Journal of Thermal Stresses 37: 292–324.

Han, X., Liu, G. R., Xi, Z. C., Lam, K. Y. (2001). Transient waves in a functionally graded cylinder, International Journal of Solids and Structures 38: 3021–3037.

Jabbari, M., Sohrabpour, S., Eslami, M. (2002). Mechanical and thermal stresses in a functionally graded hollow cylinder due to radially symmetric loads, International Journal of Pressure Vessels and Piping 79: 493–497.

Jones, I.S., Rothwell, G. (2001). Reference stress intensity factors with application to weight functions for internal circumferential cracks in cylinders, Engineering Fracture Mechanics 68: 435–454.

Lee, H. L., Chang, W. J., Sun, S. H., Yang, Y. C. (2012). Estimation of temperature distributions and thermal stresses in a functionally graded hollow cylinder simultaneously subjected to inner-and-outer boundary heat fluxes, Composites Part B: Engineering 43: 786–792.

Liew, K. M., Kitipornchai, S., Zhang, X. Z., Lim, C. W. (2003). Analysis of the thermal stress behaviour of functionally graded hollow circular cylinders, International Journal of Solids and Structures 40: 2355–2380.

MATLAB, R. "Version 8.1. 0.604 (R2013a)." Natrick, Massachusetts: The MathWorks Inc.

Meshii, T., Shibata, K., Watanabe, K. (2006). Simplified method to evaluate upper limit stress intensity factor range of an inner-surface circumferential crack under steady state thermal striping, Nuclear Engineering and Design 236: 1081–1085.

Nabavi, S.M., Ghajar, R. (2010). Analysis of thermal stress intensity factors for cracked cylinders using weight function method, International Journal of Engineering Science 48: 1811–1823.

Nami, M.R., Eskandari, H. (2012a). Three-dimensional investigations of stress intensity factors in a thermo-mechanically loaded cracked FGM hollow cylinder, International Journal of Pressure Vessels and Piping 89: 222–229.

Nami, M.R., Eskandari, H. (2012b). Three-dimensional investigations of stress-intensity factors in a cracked cylinder made of functionally graded materials, Mechanics Based Design of Structures and Machines 40: 206–217.

Nied, H., Erdogan, F. (1983). Transient thermal stress problem for a circumferentially cracked hollow cylinder, Journal of Thermal Stresses 6: 1–14.

Peng, X.-L., Li, X.-F. (2010). Transient response of temperature and thermal stresses in a functionally graded hollow cylinder, Journal of Thermal Stresses 33: 485–500.

Seifi, R. (2015). Stress intensity factors for internal surface cracks in autofrettaged functionally graded thick cylinders using weight function method, Theoretical and Applied Fracture Mechanics 75: 113-123.

Shahani, A.R., Nabavi, S.M. (2006). Closed form stress intensity factors for a semi-elliptical crack in a thick-walled cylinder under thermal stress, International Journal of Fatigue 28: 926–933.

Shahani, A.R., Nabavi, S.M. (2007). Transient thermal stress intensity factors for an internal longitudinal semi-elliptical crack in a thick-walled cylinder, Engineering Fracture Mechanics 74: 2585–2602.

Shao, Z.S., Ma, G.W. (2008). Thermo-mechanical stresses in functionally graded circular hollow cylinder with linearly increasing boundary temperature, Composite Structures 83: 259–265.

Shao, Z.S., Wang, T.J., Ang, K.K. (2007). Transient thermo-mechanical analysis of functionally graded hollow circular cylinders, Journal of Thermal Stresses 30: 81–104.

Shi, M., Wu, H., Li, L., Chai, G. (2014). Calculation of stress intensity factors for functionally graded materials by using the weight functions derived by the virtual crack extension technique, International Journal of Mechanics and Materials in Design 10: 65–77.

Shih, C.F., Moran, B., Nakamura, T. (1986). Energy release rate along a three-dimensional crack front in a thermally stressed body, International Journal of Fracture 30: 79–102.

Simulia, Dassault Systèmes, (2012). ABAQUS Documentation and User Manual. "Version 6.12." .

Walters, M.C., Paulino, G.H., Dodds Jr., R.H. (2006). Computation of mixed-mode stress intensity factors for cracks in three-dimensional functionally graded solids, Journal of Engineering Mechanics 132: 1–15.

Zhang, Y., Guo, L., Noda, N., (2014). Investigation methods for thermal shock crack problems of functionally graded materials–part II: combined analytical-numerical method, Journal of Thermal Stresses 37: 325–339.